

Superconductivity at 23 K in Pt doped BaFe₂As₂ single crystals

S. R. Saha, T. Drye, K. Kirshenbaum, N. P. Butch, and Johnpierre Paglione*
*Center for Nanophysics and Advanced Materials, Department of Physics,
University of Maryland, College Park, MD 20742, USA.*

P. Y. Zavalij

Department of Chemistry and Biochemistry, University of Maryland, College Park, MD 20742, USA.

(Dated: October 29, 2018)

We report superconductivity in single crystals of the new iron-pnictide system BaFe_{1.90}Pt_{0.10}As₂ grown by a self-flux solution method and characterized via x-ray, transport, magnetic and thermodynamic measurements. The magnetic ordering associated with a structural transition at 139 K present in BaFe₂As₂ is completely suppressed by substitution of 5% Fe with Pt and superconductivity is induced at a critical temperature $T_c = 23$ K. Full diamagnetic screening in the magnetic susceptibility and a jump in the specific heat at T_c confirm the bulk nature of the superconducting phase. All properties of the superconducting state – including transition temperature T_c , the lower critical field $H_{c1} = 200$ mT, upper critical field $H_{c2} \approx 65$ T, and the slope $\partial H_{c2}/\partial T$ – are comparable in value to the those found in other transition-metal-substituted BaFe₂As₂ series, indicating the robust nature of superconductivity induced by substitution of Group VIII elements.

PACS numbers: 74.25.Dw, 74.25.Fy, 74.25.Ha, 74.62.Dh

INTRODUCTION

The recent discovery of high-temperature superconductivity in iron-based pnictide compounds has attracted much interest among the condensed matter community, providing both a new angle for understanding the physics of unconventional superconductivity in other materials such as the copper-oxides, heavy-fermion intermetallics, etc., and an entire new family of superconducting materials of fundamental and technological interest. The highest T_c achieved so far in these materials is ~ 55 K in SmO_{1-x}F_xFeAs [1] and (Ba,Sr,Ca)FeAsF [2, 3]. Oxygen-free FeAs-based compounds with the ThCr₂Si₂-type (122) structure also exhibit superconductivity with transition temperatures reaching ~ 37 K, induced by chemical substitution of alkali or transition metal ions [4–7], the application of large pressures [8–11], or lattice strain [12].

It is widely believed that suppression of the magnetic/structural phase transition in these materials, either by chemical doping or high pressure, is playing a key role in stabilizing superconductivity in the ferropnictides [13–15]. For instance, superconductivity has been induced by partial substitution of Fe by other transition metal elements from the Fe, Co and Ni groups in both the 1111 [16–18] and 122 compounds [6, 7, 19]. For the 122 phase, superconductivity has been induced by substituting Fe with not only 3*d*-transition metals such as Co and Ni, but also some of the 4*d*- and 5*d*-transition metals. Superconductivity with T_c as high as 25 K has been observed in BaFe_{2-x}Co_xAs₂ [20, 21] and BaFe_{2-x}Rh_xAs₂ [22], and near 20 K in BaFe_{2-x}Ni_xAs₂ [15, 23] and BaFe_{2-x}Pd_xAs₂ [22] compounds. Recently, Ru and Ir substitution for Fe were

also shown to induce superconductivity in polycrystalline SrFe₂As₂ samples [24, 25], leaving only Os and Pt substitutions from the Group VIII elements uninvestigated.

Here we report the first case of superconductivity induced by Pt substitution in the FeAs-based family, presenting the observation of superconductivity at 23 K in BaFe_{1.90}Pt_{0.10}As₂. We present details of the synthesis and characterization of single crystals of this material via single-crystal x-ray diffraction, electrical resistivity, magnetic susceptibility and specific heat experiments.

EXPERIMENT

Single-crystalline samples of BaFe_{2-x}Pt_xAs₂ were grown using the FeAs self-flux method [19]. Fe and Pt were first separately pre-reacted with As via solid-state reaction of Fe (99.999%)/Pt (99.99%) powder with As (99.99%) powders in a quartz tube of partial atmospheric pressure of Ar. The precursor materials were mixed with elemental Ba (99.95%) in the ratio of FeAs:PtAs:Ba = 4 – 2*x*:2*x*:1, placed in an alumina crucible and sealed in a quartz tube under partial Ar pressure. The mixture was heated to 1150°C, slow-cooled to a lower temperature and then quenched to room temperature. Typical dimensions of as-grown single crystal specimen of BaFe_{1.90}Pt_{0.10}As₂ are 0.1 × 1 × 2 mm³. Structural properties were characterized by single-crystal X-ray-diffraction and Rietfeld refinement (SHELXS-97). Chemical analysis was obtained via both energy- and wavelength-dispersive X-ray spectroscopy, showing proper stoichiometry in all specimens reported herein and no indication of impurity phases. Resistivity (ρ) samples were prepared using gold wire/silver paint contacts made at room temperature, yielding typical contact resistances of ~ 1

Ω . Resistance measurements were performed using the standard four-probe AC method, with excitation currents of 1 mA at higher temperatures that were reduced to 0.3 mA at low temperatures to avoid self-heating, all driven at 17 Hz in a Quantum Design PPMS equipped with superconducting magnet. Magnetic susceptibility (χ) and magnetization were measured using a Quantum Design SQUID magnetometer, and specific heat was measured with a Quantum Design PPMS cryostat using the thermal relaxation method.

RESULTS

Crystallographic Parameters

Table 1 shows the crystallographic parameters determined by single-crystal X-ray-diffraction at 250 K in $\text{BaFe}_{1.90}\text{Pt}_{0.10}\text{As}_2$. A Bruker Smart Apex2 diffractometer with $\text{MoK}\alpha$ radiation, a graphite monochromator with monocarp collimator, and a CCD area detector were used for this experiment. The structure was refined with SHELXL-97 software using 1033 measured reflections of which 115 were unique and 108 observed. The final residuals were $R_1=1.95\%$ for the observed data and $wR_2=4.46\%$ for all data. Fe and Pt atoms were found to reside in the same site with a refined Fe:Pt ratio of 0.953(4):0.047(4), giving the exact formula $\text{BaFe}_{1.906(8)}\text{Pt}_{0.094(8)}\text{As}_2$ from x-ray analysis. Refinement data for BaFe_2As_2 determined by powder diffraction are adopted from Ref. [26] for comparison. As shown in Table 1, the c -axis and the c/a ratio shrink due to Pt substitution, while the a -axis and the unit cell volume expands as compared to undoped BaFe_2As_2 . Of note, the relative height of As above the Fe lattice (z -parameter) and the corresponding As-Fe-As bond angles change very little with Pt substitution.

Electrical Resistivity

Figure 1(a) presents the comparison of the in-plane resistivity $\rho(T)$ of single crystals of $\text{BaFe}_{2-x}\text{Pt}_x\text{As}_2$ with $x=0$ and 0.1 in zero applied magnetic field (data are presented after normalizing to room temperature). As shown, $\rho(T)$ data for BaFe_2As_2 exhibit metallic behavior, decreasing with temperature from 300 K before exhibiting a sharp kink at $T_0 = 139$ K, where a structural phase transition (from tetragonal to orthorhombic upon cooling) is known to coincide with the onset of antiferromagnetic (AFM) order [26]. For $x = 0$, ρ continues to decrease below T_0 without any trace of strain-induced superconductivity down to 1.8 K [12]. The drop in $\rho(T)$ below T_0 has also been observed in other 122 materials [7, 15, 20, 23], and likely arises due to the balance between the loss of inelastic scattering due to the onset

TABLE I: Crystallographic data for $\text{BaFe}_{1.90}\text{Pt}_{0.10}\text{As}_2$ determined by single-crystal x-ray diffraction. The structure was solved and refined using the SHELXS-97 software, yielding lattice constants with residual factor $R=1.95\%$. Data for BaFe_2As_2 determined by powder diffraction are adopted from Ref. [26].

	BaFe_2As_2	$\text{BaFe}_{1.90}\text{Pt}_{0.10}\text{As}_2$
Temperature	297 K	250 K
Structure	Tetragonal	Tetragonal
Space group	I4/mmm	I4/mmm
$a(\text{\AA})$	3.9625(1)	3.9772(9)
$b(\text{\AA})$	$=a$	$=a$
$c(\text{\AA})$	13.0168(3)	12.988(6)
$V^3(\text{\AA}^3)$	204.38(1)	205.45(3)
Z (formula unit/unit cell)	2	2
Density(g/cm^3)	—	6.673
Atomic parameters:		
Ba	2a(0,0,0)	2a(0,0,0)
Fe/Pt	4d(1/2,0,1/4)	4d(1/2,0,1/4)
As	4e(0,0,z)	4e(0,0,z)
	$z=0.3545(1)$	$z=0.35422(9)$
Bond lengths (\AA):		
Ba-As(\AA)	3.382(1) x 8	3.3903(10) x 8
Fe-As(\AA)	2.403(1) x 4	2.4056(8) x 4
Fe-Fe/Pt(\AA)	2.802(1) x 4	2.8123(6) x 4
Bond angles (deg):		
As-Fe-As	111.1(1) x 2	111.51(5) x 2
As-Fe-As	108.7(1) x 4	108.46(3) x 4

of magnetic order and the change in carrier concentration associated with the transition at T_0 . In the $x = 0.10$ sample, there is no indication of the T_0 transition in $\rho(T)$ down to the superconducting transition that onsets at $T_c=23$ K and drops to zero resistance by 21.5 K, indicating a resistive transition width $\Delta T_c < 1.5$ K. The suppression of the resistive superconducting transition of $\text{BaFe}_{1.90}\text{Pt}_{0.10}\text{As}_2$ with the magnetic field H applied parallel to the c -axis is illustrated in Fig. 2. The data are normalized to the normal-state resistance above T_c for clarity. Applied magnetic fields causes a tiny negative magnetoresistance at 25 K ($[\rho(H = 14 \text{ T}) - \rho(H = 0)]/\rho(H = 0) \sim -0.35\%$). The superconducting upper critical field $H_{c2}(T)$, as determined by the 50% resistive transition temperature for each field, is shown in the inset of Fig. 2. The slope $\partial H_{c2}/\partial T$ is -2.8 T/K in the range $T < 20$ K, which is comparable to values reported for other transition metal-doped FeAs-based superconductors [27]. This agreement is rather remarkable, given that these superconductors have values of T_c ranging from 10 K to more than 30 K [27]. A simple estimate using the Werthamer-Helfland-Hohenberg (WHH) approximation $H_{c2}(0) \simeq 0.691 \frac{\partial H_{c2}}{\partial T} T_c$ yields a value of ~ 45 T for the orbital $H_{c2}(0)$. However, previous studies (See Ref. [27]) have shown a more linear dependence of $H_{c2}(T)$ toward lower temperature, which would extrap-

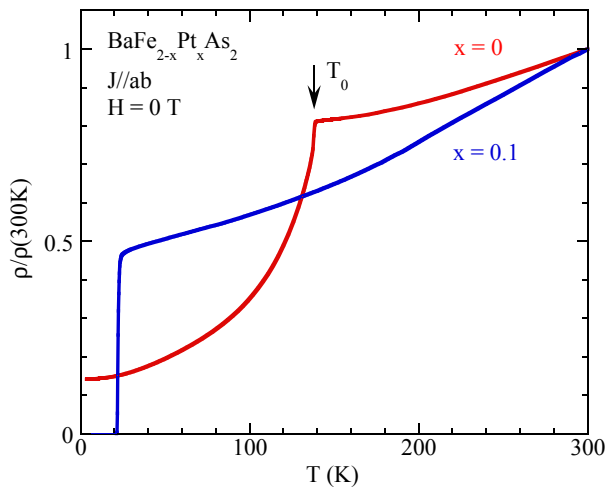


FIG. 1: Temperature dependence of in-plane electrical resistivity of $\text{BaFe}_{2-x}\text{Pt}_x\text{As}_2$ for $x=0$ and 0.1 normalized to 300 K. The arrow indicates the position of the antiferromagnetic transition associated with a structural transition at temperature T_0 , defined by the kink in $x=0$ data.

olate to a value $H_{c2}(0) \approx 65$ T for $\text{BaFe}_{1.90}\text{Pt}_{0.10}\text{As}_2$. In any case, the response of the superconducting state to applied H seems insensitive to whether superconductivity has been stabilized by different transition metals substitution, applied pressure, or presumably strain, in the case of the undoped parent compounds. In contrast, hole-doped SrFe_2As_2 and BaFe_2As_2 feature larger values of $\partial H_{c2}/\partial T$ [27].

Magnetic Susceptibility and Magnetization

Figure 3(a) presents the temperature dependence of magnetic susceptibility χ of $\text{BaFe}_{1.90}\text{Pt}_{0.10}\text{As}_2$ measured under zero-field-cooled (ZFC) conditions by applying a magnetic field of 100 mT along the ab -plane at low temperatures. As shown, χ is nearly temperature-independent down to 23 K with no indication of a magnetic/structural transition. Below 23 K, $\chi(T)$ sharply drops to negative values due to Meissner screening. The inset of Fig. 3 presents volume susceptibility $4\pi\chi$ for both at ZFC and field-cooled (FC) conditions under a 1.0 mT magnetic field applied along the ab -plane at low temperatures in order to compare the level of diamagnetic screening due to superconductivity. There is a relatively sharp drop of ZFC susceptibility from positive to negative value below $T_c=23$ K (onset) consistent with the resistivity data. As shown, the superconducting volume fraction, as estimated by the fraction of full diamagnetic screening ($4\pi\chi = -1$), reaches 100% at ~ 17 K, indicating full Meissner effect.

In order to study the magnetic response of the superconducting state, the magnetization was measured

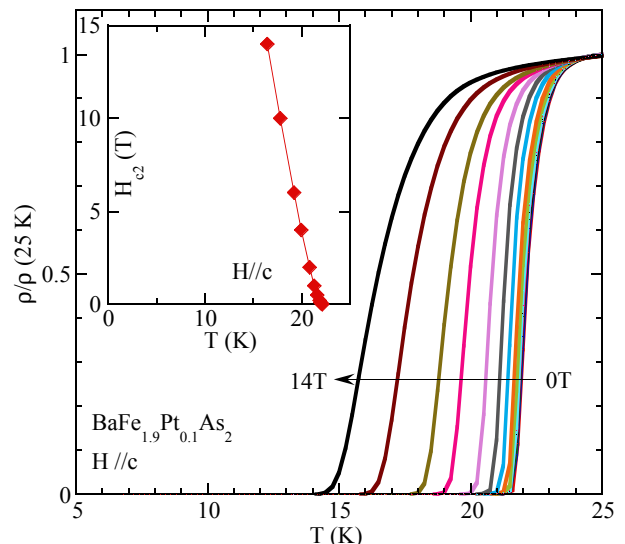


FIG. 2: In-plane electrical resistivity of $\text{BaFe}_{1.90}\text{Pt}_{0.10}\text{As}_2$ in magnetic fields ($0, 0.01, 0.02, 0.03, 0.04, 0.05, 0.1, 0.2, 0.5, 1, 2, 4, 6, 10$ and 14 T indicated by the direction of the arrow) applied along the c -axis, showing the suppression of the superconducting transition by increasing field. The resistivity is normalized to the normal state value (at 25 K) just above the transition for clarity. The inset shows upper critical field H_{c2} of $\text{BaFe}_{1.90}\text{Pt}_{0.10}\text{As}_2$, for $H \parallel c$ vs temperature. The points here denote the 50% positions of the resistive transitions for each field from the main figure.

as a function of field. Fig. 3(b) shows the isothermal ($T=1.8$ K) magnetization $M(H)$ measured from ZFC conditions. Magnetization is nonlinear and irreversible with H due to superconductivity, and it is evident that the apparent value of H_{c2} well exceeds 6 T, consistent with our resistivity studies. A minimum is observed at low H region in the virgin curve as identified by the diagonal arrow in Fig. 3(b), indicating the lower limit of a superconducting lower critical field value $H_{c1} = 200$ mT.

Specific Heat

Specific heat measurements were performed to verify the bulk thermodynamic nature of the superconducting transition in $\text{BaFe}_{1.90}\text{Pt}_{0.10}\text{As}_2$. Temperature dependent heat capacity data in zero magnetic field for $\text{BaFe}_{1.90}\text{Pt}_{0.10}\text{As}_2$ are plotted in fig. 4. An abrupt shift in the smooth $C_p(T)$ curve below 21 K, indicated by the arrow, is consistent with the superconducting phase transition observed in both resistivity and low-field magnetization data. Both the superconducting temperature and the upper critical fields in $\text{BaFe}_{1.90}\text{Pt}_{0.10}\text{As}_2$ are high, thus making a reliable estimate of the normal state electronic specific heat γ difficult. For this reason we have de-

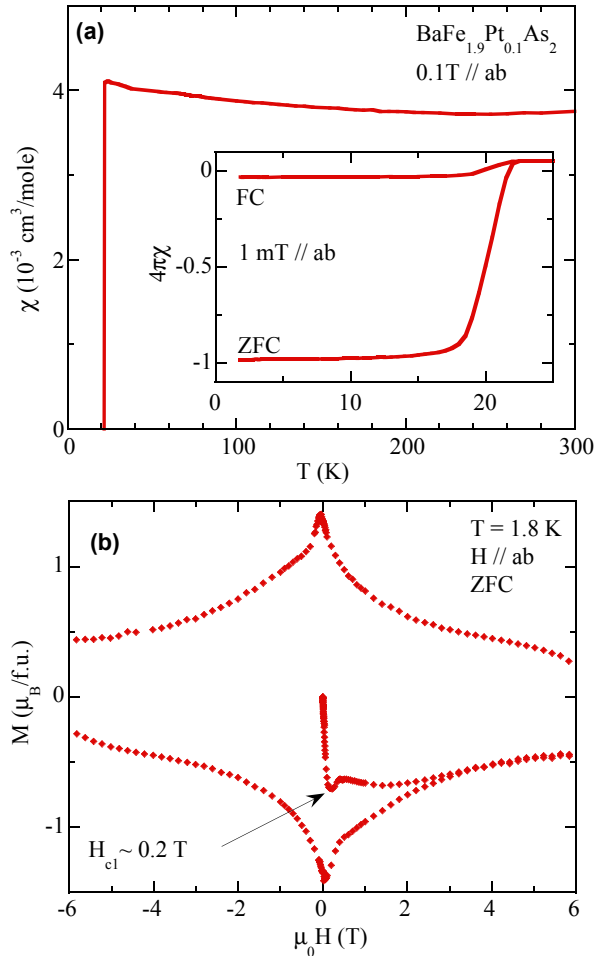


FIG. 3: (a) Temperature dependence of the magnetic susceptibility $\chi(T)$ in the $\text{BaFe}_{1.90}\text{Pt}_{0.10}\text{As}_2$ measured with 100 mT field applied parallel to the crystallographic basal plane following zero-field-cooled (ZFC) conditions. Inset: volume magnetic susceptibility at 1 mT for both ZFC and field-cooled (FC) conditions. (b) Magnetization of $\text{BaFe}_{1.90}\text{Pt}_{0.10}\text{As}_2$ as a function of applied field at 1.8 K, with H applied in-plane. The loop has a large open-ended area indicating values of H_{c2} well exceeding 6 T. Demagnetization effects due to sample geometry have been corrected for both $\chi(T)$ and $M(H)$ data.

terminated $\Delta C_p/T_c$ rather than the more traditional quantity $\Delta C_p/\gamma T_c$. Due to finite widths of superconducting transitions $\Delta C_p/T_c$ and T_c values are determined from plots of C_p/T vs T shown in the inset of fig. 4 in an enlarged view using an isoentropic construction as done previously [28]. Data for $H = 10$ T (red square symbols), in which the anomaly due to superconductivity has been shifted to lower temperature, serve as the lower line for this analysis. The vertical distance between up and down arrow gives the value of $\Delta C_p/T_c \simeq 20$ mJ/mol K. Assuming the BCS weak-coupling approximation $\Delta C_p/\gamma T_c = 1.43$ and 100% superconducting volume, the value of γ can be estimated to be about 14 mJ/mol

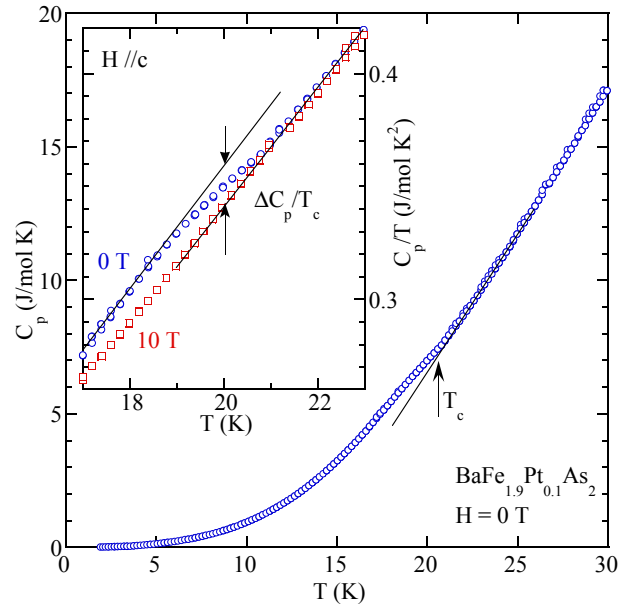


FIG. 4: Temperature-dependent heat capacity data for $\text{BaFe}_{1.90}\text{Pt}_{0.10}\text{As}_2$, showing a distinct feature centered at ~ 20 K, indicated by drawing a linear line through the data points and an upward arrow, that is consistent with the onset of superconductivity at $T_c = 23$ K determined from resistivity and magnetic susceptibility measurements. Inset: zoom of temperature dependence of C_p/T near the superconducting transition. Lines are fits to the data above and below T_c , with the arrows indicating the position where $\Delta C_p/T_c$ is determined. Data for $H = 10$ T are also plotted for comparison.

K^2 , which is comparable to that found in other transition metal-doped BaFe_2As_2 superconductors [29]. For $x = 0$ in Ref. [26], a C_p/T vs T^2 plot between 3.1 K and 14 K gives $\gamma = 16(2)$ mJ/mol K^2 corresponding to a Debye temperature of $\Theta_D = 134(1)$ K. In Ref. [28], the values of $\Delta C_p/T_c$ measured for K, Co, Ni, Rh, and Pd-doped BaFe_2As_2 superconductors have been shown to scale with T_c , regardless of the value of T_c or the relative doping position (under- or over-doped) with respect to maximum T_c . Surprisingly, the corresponding value of $\Delta C_p/T_c \simeq 20$ mJ/mol K taken at 20 K for $\text{BaFe}_{1.90}\text{Pt}_{0.10}\text{As}_2$ also falls in line with this trend, expanding this interesting relation to include another $5d$ -transition metal-doped system.

DISCUSSION

Although the detailed phase diagram is yet unknown, the superconducting properties of this new member of the superconducting FeAs-based materials look to be strikingly similar to those observed in the other related compounds. The widely perceived picture is that pairing occurs through the inter-pocket scattering of electrons via exchange of antiferromagnetic spin fluctuations [30]. By

doping electrons or holes into the parent phase, magnetic order is gradually destroyed and the short-range order provides a wide spectrum of spin fluctuations which may be responsible for pairing between electrons. Alternatively, magnetic order and superconductivity may compete to gap similar parts of the Fermi surface, with superconductivity only appearing when magnetic order is suppressed. It is certain that superconductivity is associated, directly or indirectly, with the suppression of magnetic order in the FeAs-based 122 systems, and an understanding of the generalized phase diagram must be an integral part of an explanation of the physics of these materials.

This picture can certainly give a qualitative explanation for the generally similar occurrence of superconductivity via doping of different species of Group VIII elements (including Co, Rh, Ir, Ni, Pd, and now Pt) into the 122 parent compounds. However, subtle details and differences among these different series may hold important information regarding the specific mechanism(s) by which magnetic order is suppressed and superconductivity is optimized. For instance, in $\text{BaFe}_{2-x}\text{Co}_x\text{As}_2$ the maximum T_c is found at $x \simeq 0.15$ [21, 31], whereas in $\text{BaFe}_{2-x}\text{Ni}_x\text{As}_2$ the maximum T_c occurs at approximately $x \simeq 0.10$ [15, 23]. This appears to be consistent with simple d -electron counting, and hence charge doping, however it is not clear that simple scaling of different phase diagrams by electron count works in all cases [19]. Another interesting aspect of the superconductivity in 122 materials is the similarity of maximum T_c values, typically reaching 20-25 K regardless of the transition metal substituent [25, 29]. While this is thus far true in all Ba-based compounds, the trend is broken in Sr-based 122 systems such as $\text{SrFe}_{2-x}\text{Pd}_x\text{As}_2$ [25] and $\text{SrFe}_{2-x}\text{Ni}_x\text{As}_2$ [19], which both exhibit reduced maximum values of T_c closer to ~ 10 K. While the value of T_c in $\text{BaFe}_{1.90}\text{Pt}_{0.10}\text{As}_2$ is in line with most other transition-metal doped BaFe_2As_2 superconductors, it is slightly higher than the maximum T_c of ~ 18 K found in the closely related series $\text{BaFe}_{2-x}\text{Pd}_x\text{As}_2$ [22]. Although differences in maximal T_c values could arise for many different reasons, intrinsic variations of T_c in different doping series may be an important indicator of the nature of pairing in this family of materials. Because it is known that annealing treatments of as-grown crystals of $\text{SrFe}_{2-x}\text{Ni}_x\text{As}_2$ result in a significant enhancement in superconducting transition temperatures [32], it will be important to investigate the role of crystal quality on variations in T_c values in these systems.

Finally, because Os is now the only remaining element of the Fe, Co and Ni transition metal groups to be investigated, it will be surprising if Os substitution does not also induce superconductivity in BaFe_2As_2 or SrFe_2As_2 systems. Future work will investigate this question.

SUMMARY

In summary, single crystals of the 5d-transition metal Pt-substituted BaFe_2As_2 were successfully synthesized and shown to become bulk superconductors, leaving only one remaining element in the Group VIII transition metals to be shown to induce superconductivity in the ironpnictide family of materials. Transport, magnetic and thermodynamic studies have revealed superconductivity below $T_c = 23$ K in $\text{BaFe}_{1.90}\text{Pt}_{0.10}\text{As}_2$ to be of a bulk nature and robust against applied magnetic field, with estimates of upper critical field values near ~ 65 T. The similarity in superconducting properties between the substitution series of different transition metals suggests that similar underlying physics is at play in stabilizing superconductivity in this family of materials.

ACKNOWLEDGEMENTS

The authors acknowledge B. W. Eichhorn for experimental assistance, and N.P.B. acknowledges support from a CNAM Glover fellowship. This work was supported by AFOSR-MURI Grant FA9550-09-1-0603.

* Electronic address: paglione@umd.edu

- [1] Ren Z -A, Lu W, Yang J, Yi W, Shen X -L, Zheng-Cai, Che G -C, Dong X -L, Sun L -L, Zhou F, and Zhao Z -X, 2008 *Chin. Phys. Lett.* **25** 2215.
- [2] Zhu X, Han F, Cheng P, Mu G, Shen B, and Wen H H, 2009 *Europhys. Lett.* **85** 17011.
- [3] Cheng P, Shen B, Mu G, Zhu X, Han F, Zeng B, and Wen H H, 2009 *Euro Phys. Lett.* **85** 67003.
- [4] Sasmal K, Lv B, Lorenz B, Guloy A M, Chen F, Xue Y -Y, and Chu C -W, 2008 *Phys. Rev. Lett.* **101** 107007.
- [5] Rotter M, Tegel M, and Johrendt D, 2008 *Phys. Rev. Lett.* **101** 107006.
- [6] Sefat A S, Jin R, McGuire M A, Sales B C, Singh D J, and Mandrus D, 2008 *Phys. Rev. Lett.* **101** 117004.
- [7] Leithe-Jasper A, Schnelle W, Geibel C, and Rosner H, 2008 *Phys. Rev. Lett.* **101** 207004.
- [8] Torikachvili M S, Bud'ko S L, Ni N, and Canfield P C, 2008 *Phys. Rev. Lett.* **101** 057006.
- [9] Park T, Park E, Lee H, Klimczuk T, Bauer E D, Ronning F, and Thompson J D, 2008 *J. Phys.: Condens. Matt.* **20** 322204.
- [10] Alireza P L, Chris-Ko Y T, Gillett J, Petrone C M, Cole J M, Lonzarich G G, and Sebastian S E, 2009 *J. Phys.: Condens. Matt.* **21**, 012208.
- [11] Kumar M, Nicklas M, Jesche A, Caroca-Canales N, Schmitt M, Hanfland M, Kasinathan D, Schwarz U, Rosner H, and Geibel C, 2008 *Phys. Rev. B* **78** 184516.
- [12] Saha S R, Butch N P, Kirshenbaum K, and Paglione Johnpierre, 2009 *Phys. Rev. Lett.*, **103** 037005.
- [13] Lee C -H, Iyo A, Eisaki H, Kito H, Fernandez-Diaz M T, Ito T, Kihou K, Matsuhata H, Braden M, and Yamada K, 2008 *J. Phys. Soc. Jpn.* **77** 083704.

- [14] Kreyssig A, Green M A, Lee Y, Samolyuk G D, Zajdel P, Lynn J W, Bud'ko S L, Torikachvili M S, Ni N, Nandi S, J B Leao, Poulton S J, Argyriou D N, Harmon B N, McQueeney R J, Canfield P C, and Goldman A I, 2008 *Phys. Rev. B* **78** 184517.
- [15] Canfield P C, Bud'ko S L, Ni N, Yan J Q, Kracher A, 2009 *Phys. Rev. B* **80** 060501(R).
- [16] Sefat A S, Huq A, McGuire M A, Jin R, Sales B C, Mandrus D, Cranswick L M D, Stephens P W, and Stone K H, 2008 *Phys. Rev. B* **78** 104505.
- [17] Wang C, Li Y K, Zhu Z W, Jiang S, Lin X, Luo Y K, Chi S, Li L J, Ren Z, He M, Chen H, Wang Y T, Tao Q, Cao G H, and Xu Z A, 2009 *Phys. Rev. B* **79** 054521.
- [18] Cao G, Jiang S, Lin X, Wang C, Li Y, Ren Z, Tao Q, Feng C, Dai J, Xu Z A, Zhang F -C, 2009 *Phys. Rev. B* **79** 174505.
- [19] Saha S R, Butch N P, Kirshenbaum K, and Paglione Johnpierre, 2009 *Phys. Rev. B* **79** 224519.
- [20] Ni N, Tillman M E, Yan J -Q, Kracher A, Hannahs S T, Budko S L, and Canfield P C, 2008 *Phys. Rev. B* **78**, 214515.
- [21] Chu J -H, Analytis J G, Kucharczyk C, and Fisher I R, 2009 *Phys. Rev. B* **79** 014506.
- [22] Ni N, Thaler A, Kracher A, Yan J -Q, Budko S L, and Canfield P C, 2009 *Phys. Rev. B* **80** 024511.
- [23] Li L J, Wang Q B, Luo Y K, Chen H, Tao Q, Li Y K, Lin X, He M, Zhu Z W, Cao G H, and Xu Z A, 2009 *New J. Phys.* **11** 025008.
- [24] Schnelle W, Leithe-Jasper A, Gumenuik R, Burkhardt U, Kasinathan D, Rosner H, 2009 *Phys. Rev. B* **79** 214516.
- [25] Han F, Zhu X, Cheng P, Mu G, Jia Y, Fang L, Wang Y, Luo H, Zheng B, Shan L, Ren C, Wen H H, 2009 *Phys. Rev. B.* **80** 024506.
- [26] Rotter M, Tegel M, Johrendt D, Schellenberg I, Hermes W, and Pöttgen R, 2008 *Phys. Rev. B* **78** 020503(R).
- [27] Butch N P, Saha S R, Zhang X, Kirshenbaum K, Greene R and Paglione Johnpierre, 2010 *Phys. Rev. B* **81** 024518.
- [28] Bud'ko S L , Ni N, and Canfield P C, 2009 *Phys. Rev. B* **79** 220516(R).
- [29] Ni N, Thaler A, Yan J-Q, Kracher A, Budko S L, and Canfield P C, 2009 *Phys. Rev. B* **80** 214511.
- [30] Mazin I I, Schmalian J, 2009 *Physica C* **469** 614.
- [31] Wang X F, Wu T, Wu G, Liu R H, Chen H, Xie Y L and Chen X H, 2009 *New J. Phys.* **11** 045003.
- [32] Saha S R, Butch N P, Kirshenbaum K, and Paglione J, 2010 *Physica C* at press (arXiv:0908.4095).